Computing Clinically Relevant Binding Free Energies of HIV-1 Protease Inhibitors

David W. Wright,[†] Benjamin A. Hall,[†] Owain A. Kenway,[†] Shantenu Jha,[‡] and Peter V. Coveney[*,†]

Centre for Computational Science, Department of Chemistry,University College London, London, WC1H 0AJ, U.K., and Electrical and Computer Engineering, Rutgers, Piscataway, NJ 08854, U.S.A.

E-mail: p.v.coveney@ucl.ac.uk

Abstract

The use of molecular simulation to estimate the strength of macromolecular binding free energies is becoming increasingly widespread, with goals ranging from lead optimisation and enrichment in drug discovery to personalizing or stratifying treatment regimes. In order to realize the potential of such approaches to predict new results, not merely to explain previous experimental findings, it is necessary that the methods used are reliable and accurate, and that their limitations are thoroughly understood. However, the computational cost of atomistic simulation techniques such as molecular dynamics (MD) has meant that until recently little work has focussed on validating and verifying the available free energy methodologies, with the consequence that many of the results published in the literature are unreproducible. Here we present a detailed analysis of two of the most popular approximate methods for calculating binding free energies from molecular simulations, molecular mechanics Poisson-Boltzmann

[*]To whom correspondence should be addressed
[†]University College London
[‡]Rutgers

surface area (MMPBSA) and molecular mechanics generalized Born surface area (MMGBSA), applied to the 9 FDA approved HIV-1 protease inhibitors. Our results show that the values obtained from replica simulations of the same protease - drug complex, differing only in initially assigned atom velocities, can vary by as much as 10 kcal mol^{-1}, which is greater than the difference between the best and worst binding inhibitors under investigation. Despite this, analysis of ensembles of simulations producing 50 trajectories of 4 ns duration leads to well converged free energy estimates. For 7 inhibitors we find that with correctly converged normal mode estimates of the configurational entropy we can correctly distinguish inhibitors in agreement with experimental data for both the MMPBSA and MMGBSA methods and thus have the ability to rank the efficacy of binding of this selection of drugs to the protease (no account is made for free energy penalties associated with protein distortion leading to the over estimation of the binding strength of the two largest inhibitors ritonavir and atazanavir). Our work provides a thorough assessment of what is required to produce converged and hence reliable free energies for protein-ligand binding.

1 Introduction

In the last two decades both computationally assisted rational drug design and personalized medicine have been held out as potential new paradigms which would produce new therapies at a time when the approval of new drugs is in seemingly irreversible decline[1,2]. One of the key components of these approaches is the need for predictive modelling of protein function and binding selectivity. Consequently, delivering on the promises made for each requires that the tools used in basic research are fully validated and their range of applicability both understood and acknowledged.

From a physical perspective the quantity which governs biomolecular association, determining whether proteins bind to one another or ligands (where the latter may be natural or pharmaceutical in origin), is the binding affinity. Consequently, the calculation of binding free energies (also known as 'binding affinities') is one of the most important areas of biomolecular simulation. One of the most widely applied simulation techniques in this field is molecular dynamics (MD)[3,4],

in which the motions of the atoms that make up proteins are computed using a simplified model based on Newtonian mechanics. Theoretically, the accuracy of the estimates of any thermodynamic quantity from MD is limited by two factors: that of the forcefields used to describe the inter-atomic interactions and the inability to sample sufficiently the ensemble of microstates available to the system.

A variety of approaches are available for calculating binding affinities from MD simulations ranging from the theoretically rigorous, such as thermodynamic integration (TI) or umbrella sampling (US), to the largely empirical, such as the linear interaction energy (LIE) method (excellent reviews of this subject are available by Gilson and Zhou[5], and Steinbrecher and Labahn[6]). The computational requirements of these methods tends to increase considerably as more physical detail is included in the models used. In both drug discovery, where large numbers of candidates must be assessed, and clinical applications, where diagnoses must typically be given in days or at most weeks, rapid turn around of calculations is vital and calculations that take a week or more to complete are unlikely to ever be adopted beyond basic research environments. More fundamentally, it is not the notional accuracy of the different methods but the reproducibility of the results obtained which needs to be verified and validated before any method can be seen as a reliable tool for future applications.

The molecular mechanics Poisson-Boltzmann surface area (MMPBSA)[7,8] and molecular mechanics generalized Born surface area (MMGBSA)[9] methods of estimating binding free energies have become some of the most widely applied due to their claims to provide a compromise between accuracy and speed. Both of these methods, however, neglect to account for changes in configurational entropy upon binding. Consequently, they are frequently combined with estimates of this contribution made using normal mode analysis of harmonic frequencies from minimized snapshots from the MD trajectory. Whilst the convergence and applicability of MMPBSA and MMGBSA have been widely studied[10,11] the computational cost of normal mode analysis has meant that only recently has its performance begun to be similarly investigated[12]. Here we present an extensive analysis of the convergence properties and ability to reproduce experimental values of

the methods applied to HIV-1 protease binding to the nine FDA approved inhibitors. These results build on our previous work that used these techniques to evaluate differences in binding strength of different protein sequences to individual drugs in both the HIV protease[13,14] and the anti-cancer therapy target epidermal growth factor receptor (EGFR)[15]. In the latter case the prediction made for the L858R mutant was thought to disagree with experimental results[16] but more recent data have confirmed the validity of the computational estimates[17].

Ensembles of multiple short simulations were run for each protein-ligand combination as previous studies have suggested that a multiple/ensemble MD approach can sample phase space more efficiently than fewer long time simulations[13,18,19]. This approach also allows us to investigate the reproducibility of the calculations on the individual simulations within an ensemble (we will refer to an individual simulation within an ensemble for each inhibitor as a replica). We also evaluate the performance of a significantly less computationally expensive method proposed by Swanson et al.[20] for accounting for neglected terms in the MMPBSA/MMGBSA methods using the MD trajectories directly.

2 Methods

When two reactants combine at constant temperature and pressure the binding affinity is characterized by the change in Gibbs free energy given by

$$\Delta G = \Delta H - T\Delta S \tag{1}$$

at temperature T and is composed of the change in enthalpy (ΔH) and the change in entropy (ΔS). In this study we aim to assess the ability of several different end-point free energy calculation methodologies to estimate ΔG using protein-ligand conformations generated via molecular dynamics simulations. The methods under investigation are MMPBSA[7,8] and MMGBSA including and excluding terms aiming to explicitly incorporate solute entropic contributions to the binding energy. All of these methods run as post processing steps on snapshots taken from the MD trajec-

tories, with averages computed over all snapshots.

Even incorporating terms describing solute entropic contributions these methods possess several apparent limitations for computing absolute binding free energies. They do not implicitly account for free energy differences that arise from possible changes in key protonation states or explicit water-mediated binding between protein and ligand which may provide significant contributions to the binding free energy[21]. Despite these limitations and scepticism about the validity of the methods in some quarters[22], our previous work indicates that changes in binding energy of less than 1 kcal mol^{-1} between HIV-1 protease mutants can be distinguished[13,23].

2.1 Free Energy Calculation Protocols

Both MMPBSA and MMGBSA are endpoint free energy calculations. In such methods the free energy of binding, ΔG is calculated using:

$$\Delta G = \langle G_{complex} \rangle - \langle G_{enzyme} \rangle - \langle G_{ligand} \rangle , \tag{2}$$

where $\langle G_{complex} \rangle$, $\langle G_{enzyme} \rangle$ and $\langle G_{ligand} \rangle$ are the average values of the Gibbs free energy for the complex, enzyme and ligand respectively. Separate simulation of the complex and its two components can be used but due to difficulties in obtaining free energies it is more common to extract configurations of the free enzyme and ligand from simulation of the complex. This is the strategy we have employed in the present. Normal mode solute entropy calculations use the same configurations and also a calculation similar to Eq. (2) to compute the overall entropic penalty from values computed for the complex, enzyme and ligand. The free energy of association, however, deals exclusively with the degrees of freedom available to the bound ligand and is computed from collections of snapshots. The details of all four computations are provided below.

2.1.1 MMPBSA and MMGBSA

The binding free energy change calculated by MMPBSA and MMGBSA ($\Delta G_{MMPB(GB)SA}$) can be broken down into a number of components:

$$\Delta G_{MMPB(GB)SA} = \Delta G^{MM}_{ele} + \Delta G^{MM}_{vdW} + \Delta G^{MM}_{int} + \Delta G^{sol}_{nonpol} + \Delta G^{sol}_{pol} \quad (3)$$

where ΔG^{MM}_{vdW} and ΔG^{MM}_{ele} are the van der Waals and electrostatic contributions to the molecular mechanics free energy difference, respectively, and ΔG^{sol}_{pol} and ΔG^{sol}_{nonpol} are the polar and non-polar solvation terms, respectively. Modules of the AMBER 9 package[24] were used in the evaluation of all components of the MMPBSA calculation. The SANDER module was employed to calculate both molecular mechanics terms (ΔG^{MM}_{vdW} and ΔG^{MM}_{ele}), with no cut-off being applied to the non-bonded energies. The electrostatic free energy of solvation, ΔG^{sol}_{pol}, is the part of the calculation described by the Poisson-Boltzmann (PB) or generalized Born (GB) calculation. GB is an approximation to PB and in both methods internal and external dielectric constants of 1 and 80 were used respectively. In the PB case, a thousand iterations of the linear Poisson-Boltzmann equation were performed on a cubic lattice grid with a spacing of 0.5 Å using the DelPhi[25] program. The GB calculations were calculated using the model proposed by Onufriev et al.[9]. The non-polar solvation energy, ΔG^{sol}_{nonpol}, was calculated from the solvent accessible surface area (SASA) using the MSMS program[26] with a 1.4 Å radius probe based on the equation:

$$\Delta G^{sol}_{nonpol} = \gamma A + \beta, \quad (4)$$

where A is the solvent accessible surface area difference, γ is the surface tension and β the offset. The constants γ and β were set to the standard values of 0.0052 kcal mol^{-1}Å^{-2} and 0.92 kcal mol^{-1}, respectively in our MMPBSA simulations and 0.0072 kcal mol^{-1}Å^{-2} and 0 kcal mol^{-1} in MMGBSA[7–9].

2.1.2 Normal Mode Analysis

The non-polar solvation term of the MM(GB)PBSA calculation incorporates an implicit estimate of the entropic changes associated with the insertion of a solute into the solvent. However, no account is made for the entropic impact of changes in the configurational freedom of the enzyme and ligand upon complex formation *in vacuo*. In general, protein-ligand binding events cause restrictions to the number of conformations available to both and consequently a reduction in entropy; this contribution is known as the configurational (or conformational) entropy. For some systems it has been observed that agreement with experimental binding affinity values can be improved by incorporating a normal mode estimation of the entropic component of the binding free energy alongside MMPB(GB)SA[13,27]. Including this contribution the final binding affinity estimate ΔG_{theor} is given by:

$$\Delta G_{theor-PB(GB)} = \Delta G_{MMPB(GB)SA} - T\Delta S_{NM} \tag{5}$$

where $\Delta G_{MMPB(GB)SA}$ is the MMPBSA or MMGBSA binding affinity estimate, T the thermodynamic temperature and $-T\Delta S_{NM}$ is the normal mode estimate of the configurational entropy penalty of the binding reaction.

2.1.3 Free Energy of Association

Swanson et al.[20] proposed a method for improving the validity of MMPBSA binding energy calculations which they called the free energy of association (which we will denote using ΔG_{Assoc}); this is simply added to the MMPB(GB)SA value:

$$\Delta G_{PB(GB)-Assoc} = \Delta G_{MMPB(GB)SA} + \Delta G_{Assoc}. \tag{6}$$

ΔG_{Assoc} is conceptually linked to the freedom of motion which is left to the ligand upon binding and provides a previously lacking link between the estimated binding affinity and the standard

concentration. The term is computed from:

$$\Delta G_{Assoc} = -RT \ln \left(\frac{C^o z_{lig}^{trans} z_{lig}^{rot}}{8\pi^2} \right), \tag{7}$$

where C^o is the standard state concentration, usually taken to be 1 M (1 molecule/1660 Å^3), z_{lig}^{trans} and z_{lig}^{rot} are the ligand translational and rotational configuration integrals, respectively.

z_{lig}^{trans} was calculated by superimposing every snapshot onto an average structure of the protease using C_α atoms alone. This provides a static reference system along with an average ligand structure. The eigenvalues (λ_i) of the covariance matrix of the ligand center of mass were then computed providing variance measures along three independent axes from the relation the $\lambda_i = < \Delta x_i^2 >$. The translational configurational integral is then given by:

$$z_{lig}^{trans} = (2\pi)^{3/2} (< \Delta x_1^2 >< \Delta x_2^2 >< \Delta x_3^2 >)^{1/2} \tag{8}$$

Similarly, the ligand's rotational integral can be computed from quaternions representing the ligand's rotational motion relative to the average structure. A small angle approximation allows the reduction of the three quaternions describing rotation about three axes into a single quaternion, three of whose components are sinusoidally related to three rotation angles. As for the translational component, the covariance matrix can be evaluated to produce eigenvalues that can be used to calculate z_{lig}^{rot} in an analogous manner to Eq. (8).

The structural superposition of each snapshot onto the average structure was performed using scripts based on the alignment code found in MDAnalysis[28–30]. The use of this method is attractive as it is based on the configurations taken directly from the simulations and is computationally inexpensive. This method assumes that the simulation explores a single minimum, whereas we expect that replicas will explore different minima. Consequently, here we evaluate ΔG_{Assoc} for each replica individually.

2.2 Model Preparation and Simulation Protocol

Preparation and simulation set up was performed using the automated Binding Affinity Calculator (BAC) tool (full details of the tool and the simulation parameters employed are available in[31]). Models of the subtype B HXB2 wildtype sequence of HIV-1 were constructed using the coordinates from PDB crystal structures listed in Table 1. All systems were solvated in orthorhombic water boxes with a minimum extension from the protein of 14 Å.

Table 1: The PDB codes of the crystal structures used to provide coordinates for the HIV-1 bound to each of the nine FDA approved protease inhibitors.

Drug Name	**Abbreviation**	**PDB**
Amprenavir	APV	1HPV
Atazanavir	AZV	2AQU
Darunavir	DRV	2HSI
Indinavir	IDV	1HSG
Lopinavir	LPV	1MUI
Nelfinavir	NFV	1OHR
Ritonavir	RTV	1HXW
Saquinavir	SQV	1FB7
Tipranavir	TPV	2O4P

Protein parameters were taken from the standard AMBER forcefield for bioorganic systems (ff03)[32]. Drug parameters were produced using the general AMBER forcefield (GAFF)[33] following the procedure detailed in Sadiq et al.[31] with the exception that drug protonation states were determined using Open Babel[34] (using a pH of 5, based upon the conditions used in most binding assays for the protease). Gaussian 98[35] was used to perform geometric optimization of the inhibitor, with 6-31G** basis functions and the restrained electrostatic potential (RESP) procedure, also part of the AMBER package, was used to calculate the partial atomic charges. All ligands were found to be neutral except for Indinavir which was protonated at pH 5, in agreement with the previous findings of Oehme et al.[12] (structures for all 9 inhibitors are shown in Figure 1). Before the production simulations reported here were run, all systems were minimised and equilibrated for 2 ns using the protocol defined by the BAC[31].

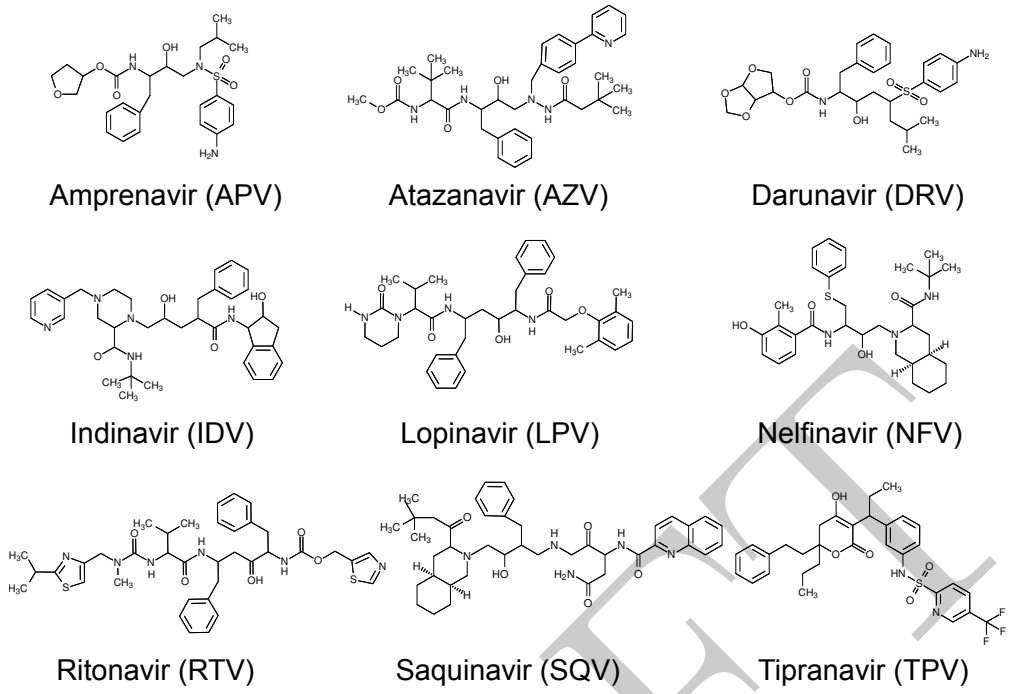

Figure 1: The chemical structures of all 9 FDA approved protease inhibitors simulated in this study.

All simulations presented here were performed in the molecular dynamics package NAMD2[36] in the NPT ensemble with a temperature of 300 K and a pressure of 1 bar, using a 2 fs time step. Free energy analysis was conducted on configuration snapshots generated over the course of MD simulations using the NMODE and MMPBSA modules of the AMBER 9 package[24]. Snapshots were output every 10 picoseconds to give 100 snapshots per nanosecond of simulation. Management of ensemble simulation runs and analysis was facilitated by use of the BigJob[37,38] extension of the SAGA middleware[39], further details of which are provided in Supporting Information.

The HIV-1 protease consists of two peptide chains, which are usually constructed from the same sequence of amino acids (the structure of the drug bound protein is shown in Figure 2). The catalytic function of the enzyme is performed by a dyad which consists of two aspartic acid (Asp) residues, one in position 25 of each chain (we label that in the first chain D25 and that in the second D25′). It has been established by our group and others that the correct determination of the protonation state of the catalytic dyad of HIV-1 protease is of vital importance in order to obtain accurate binding affinities[13,40]. Four possible protonation states are possible for the system dianionic (D-), diprotonated (D25, D25′), Asp 25 protonated (D25), and Asp 25′ protonated (D25′).

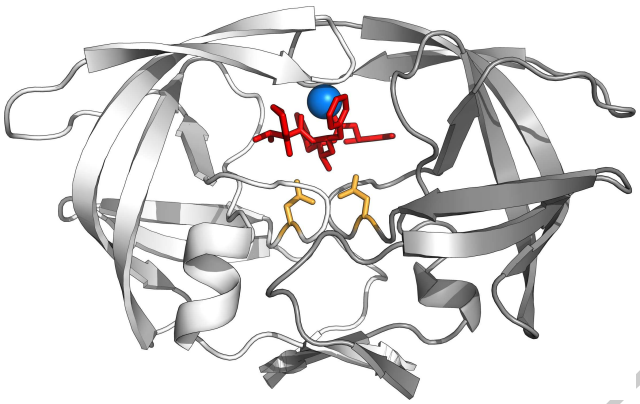

Figure 2: Structure of the lopinavir bound HIV-1 protease (shown in cartoon representation). The two monomers are shown in white and grey, with the inhibitor lopinavir and the catalytic dyad at position 25 of each protease monomer in chemical structure representation (in red and orange respectively). The conserved water molecule bound between the inhibitor and protease flaps is shown in blue.

We have employed the same protocol used previously to establish the protonation state appropriate for lopinavir (LPV)[13] in order to ascertain the correct protonation state for each drug. Twenty replica simulations (varying only in having different, randomised initial velocities) were performed for each system. Each simulation produced 2 ns of equilibration and 4 ns of production trajectory. In all cases except Tipranavir, where the diprotonated system was favoured, the protein was found to be monoprotonated. Full results for each system are given in Table S1.

Once the correct catalytic dyad protonation state was determined for each drug, 30 more replicas were performed for all systems using the same conditions and the binding affinity averages calculated from the full 50 member ensembles used for our final comparison of drug binding affinities. This size of ensemble was shown to provide well converged ΔG_{MMPBSA} results for protease mutants bound to the inhibitor lopinavir in our previous work[13]. A second ensemble of the lopinavir system was run and analysed in order to assess the reproducibility of the binding affinity estimates produced (the second ensemble is denoted as LPV 2).

3 Results

Our aim in the following sections is to investigate both the level of conformational sampling required to obtain converged results and, once this has been ascertained, to compare the performance of the different methods of free energy calculation in terms of how well they reproduce experimental results.

3.1 Internal Sampling, Convergence, and Reproducibility

The combination of the computational cost of the calculations and the necessity for rapid results in applications such as drug discovery and lead enrichment has led many previous studies of MMPBSA and MMGBSA performance to be limited to single simulations, often providing less than 10 ns of MD trajectory for analysis[10–12]. Here we use ensembles of 50 simulations to determine the variability of the results produced by these analyses and how they depend upon the replica length and rate at which conformational samples are taken from the MD trajectories. This strategy is enabled by the increasing availability of supercomputing resources with many thousand of cores (some times referred to as petascale resources) which make the execution of many large simulations feasible. In this work we harnessed resources on both the US XSEDE and EU PRACE networks (details of the machines used can be found in the Supporting Information).

3.1.1 Effect of Simulation Length and Sampling Rate

Our previous work suggested that ensembles of 50 replica simulations producing 4 nanoseconds of production trajectory were capable of producing well converged MMPBSA values and to correctly rank a series of protease mutants bound to lopinavir (LPV) but that longer single simulations could not[13]. More recent work has suggested that single simulations of 10 nanosecond duration can produce reliable results using MMPBSA for a selection of 14 HIV-1 protease inhibitors selected to give a wide range of affinities and to include representative of six different scaffolds they identified from the literature[11]. Here we focus on using 50 replica ensembles to see if we can extend our

previous analysis to cover all of the FDA approved HIV-1 protease inhibitors. In order to assess the impact of replica simulation length and sampling rate on the convergence of averages obtained by each of the free energy protocols under study a method to quantify the error in the averages taken from a given ensemble is required. We have chosen to use the statistical technique of bootstrapping[41]. This method involves resampling with replacement the N input data points (in this case the snapshot values of ΔG_{MMPBSA}, ΔG_{MMGBSA} or $-T\Delta S_{NM}$) to provide a new bootstrap sample also containing N data points. This process is repeated many times (in our case 10,000 times) and the mean of each bootstrap population calculated. The standard deviation (σ_{boot}) of these means provides an estimate of the error associated with an average derived from a given sample.

Figure 3 shows the variation of σ_{boot} with replica length and sampling rate for ΔG_{MMPBSA} ΔG_{MMGBSA} and $-T\Delta S_{NM}$ in the case of the wildtype protease bound to lopinavir (LPV). The most surprising feature of these tracks is that after 4 nanoseconds σ_{boot} increases for both ΔG_{MMPBSA} and ΔG_{MMGBSA} despite the increased level of sampling being used. This is particularly pronounced for ΔG_{MMPBSA} and is due to the ingress of water into the active site as identified in our previous work[13,14,42] leading to higher variability in MMPBSA results. The results for ΔG_{MMGBSA} already appear very well converged at the 4 nanosecond point with a σ_{boot} of less than 0.21 kcal mol^{-1}at all of the sampling rates investigated; in the case of ΔG_{MMPBSA} the error is less than 0.3 kcal mol^{-1}at this trajectory length. We have therefore limited all of the remaining replica lengths to 4 nanoseconds. There is little benefit observable for either method when the sampling rate is increased above 20 snapshots per nanosecond. Despite this, for reasons of consistency with our previous work we have used 100 snapshots per nanosecond for our ΔG_{MMPBSA} and ΔG_{MMGBSA} averages.

Figure 3(c) shows that, unlike for ΔG_{MMPBSA}, the error on $-T\Delta S_{NM}$ averages is significantly reduced as the sampling rate increases up to a maximum of 100 snapshots per nanosecond. Here there is no sign of any change in the convergence behaviour as the length of simulation produced by each replica is increased. In order to have comparable error levels at reasonable computational cost we have chosen to use 25 snapshots per nanosecond for $-T\Delta S_{NM}$ calculations which provide an estimated error σ_{boot} of approximately 0.3 kcal mol^{-1}, comparable to those obtained for ΔG_{MMPBSA}.

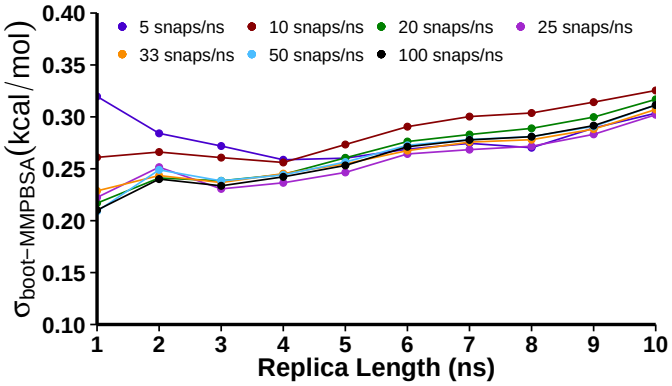

(a)

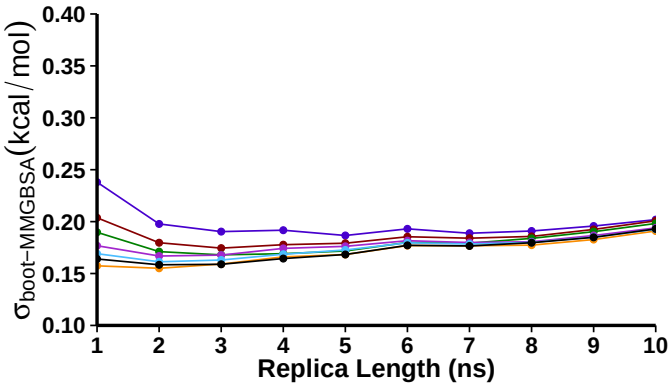

(b)

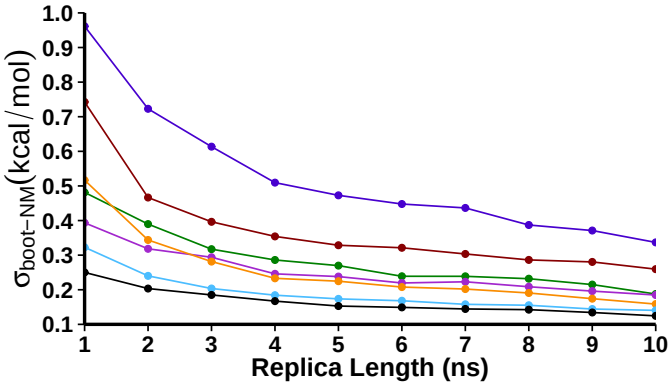

(c)

Figure 3: The variation of the bootstrap statistics, σ_{boot}, with replica simulation length and the sampling rate used for the averages of (a)ΔG_{MMPBSA}, (b) ΔG_{MMGBSA}, and (c) $-T\Delta S_{NM}$ for 50 replica ensemble simulations of wildtype HIV-1 protease bound to the inhibitor LPV.

3.1.2 Variance Between Replicas

Given that the vast majority of publications that apply the MMPBSA or MMGBSA methodologies report no more than one or two simulations, it is instructive to examine the variation in binding free energy values we observe from different replica simulations. Figures 4(a) and 4(c) show the distribution of the averages obtained for each replica via the MMPBSA and MMGBSA methodologies respectively. The distributions are very broad for all combinations of drug and methodology, in almost every case (excepting NFV using MMGBSA and one of the LPV replicas using MMPBSA) the range of values observed being greater that 7 kcal mol^{-1}. Using both methodologies the values for AZV and RTV have the largest ranges, all of which exceed 10 kcal mol^{-1}. In addition to the width of these distributions it is clear from visual inspection that the results do not fit well to the expected Gaussian distribution, which would seem to indicate that sampling on this level is not well converged. By contrast the ΔG_{MMPBSA} and ΔG_{MMGBSA} snapshot distributions, shown in Figure 4(b) and Figure 4(d) respectively, do appear to follow well defined Gaussian distributions. We suggest that the latter observation and the fact that the distributions for the two LPV replicas lie very close together mean that the overall averages are well converged even if this is not clear from the replica distributions.

A similar result is obtained for normal mode estimates of the configurational entropy, albeit with a much larger range in the snapshot values obtained. Again, the snapshot based normalized frequency distributions of the values closely resemble normal distributions with the same mean and standard deviation as shown in Figure 5(b). This is a significant result as, previously, we were unable to obtain the expected Gaussian distribution of values when using a lower sampling rate of 5 snapshots per nanosecond for a total of 1,000 snapshots per ensemble (here we use 5,000).[13] The computational cost of normal mode analysis has meant that many published studies use far fewer snapshots than this. In all cases the distributions are very broad, the range of values is greater than 80 kcal mol^{-1}, and encompass some snapshots with attractive (negative) contributions to the binding free energy. As for the MMPB(GB)SA results the replica averages do not produce well defined normal distributions. However, in line with the bootstrap analysis presented above, the replica dis-

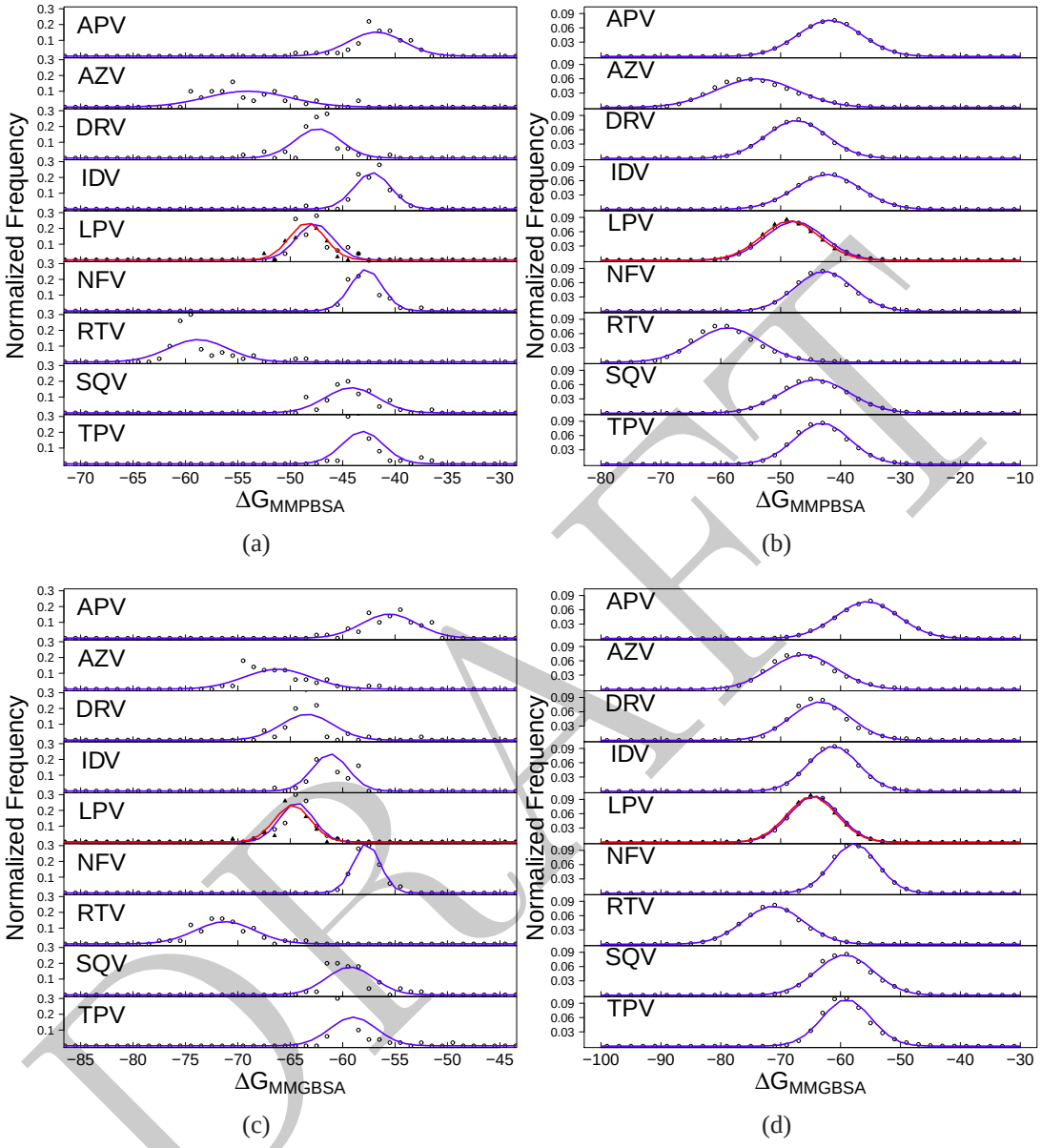

Figure 4: Normalized frequency distribution analysis of the binding affinities. Distributions for MMPBSA (ΔG_{MMPBSA}) are shown in (a) per replica averages and (b) per snapshot and those for MMGBSA (ΔG_{MMGBSA}) in (c) per replica average and (d) per snapshot for each of the 9 protease inhibitors studied. In the case of the inhibitor lopinavir (LPV) two replica ensembles are shown, the first with open circles and the latter filled triangles. Explanations of the abbreviations used for each drug are given in Table 1. The expected normal distribution given the same mean and standard deviation for each dataset is shown by the blue lines (the distribution for the second LPV replica is shown in red).

tributions are only seen to be as broadly distributed as those for the MMPB(GB)SA results. This confirms that by using 25 snapshots per replica we are able to produce well converged estimates of the configurational entropy. It is not possible to produce consistent per snapshot distributions of $\Delta G_{theor-PB}$ or $\Delta G_{theor-GB}$, due to the differences in sampling rate, but per replica distributions show similar deviations and have a comparable range to those of ΔG_{MMPBSA} and ΔG_{MMGBSA} (see Figure 6). The narrowest replica distribution for the ΔG_{MMPBSA} and ΔG_{MMGBSA} results (for NFV and LPV respectively) have a standard deviation of 1.5 and 1.6 kcal mol^{-1}, while those for $\Delta G_{theor-PB}$ and $\Delta G_{theor-GB}$ (TPV and LPV respectively) are 2.22 and 2.48 kcal mol^{-1}. The two largest drugs under investigation, RTV and AZV, have consistently broader distributions than the others using either MMPBSA or MMGBSA, with or without the incorporation of $-T\Delta S_{NM}$.

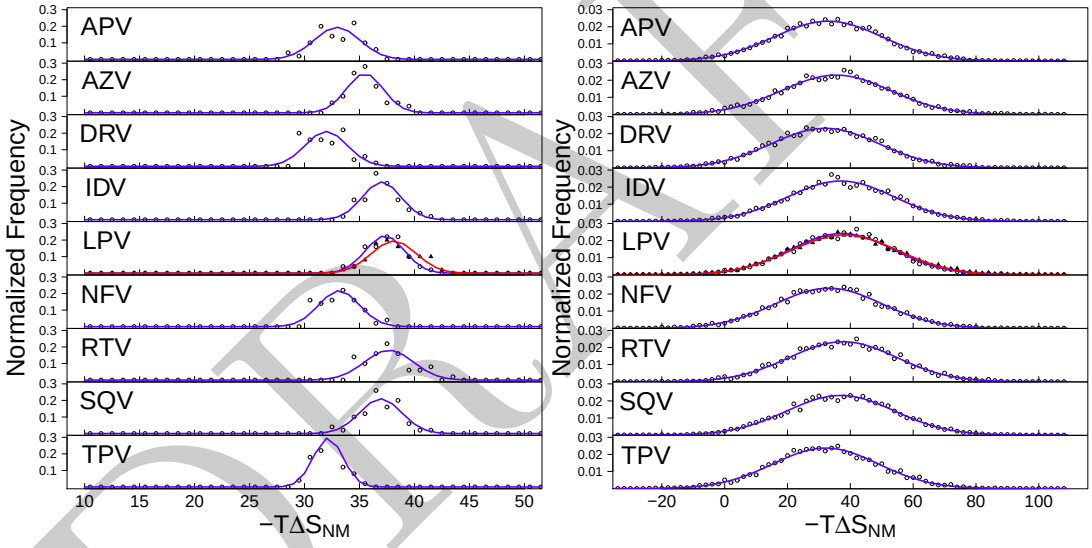

Figure 5: Normalized frequency distribution analysis of the conformational entropy contribution to the binding affinities ($-T\Delta S_{NM}$) calculated for (a) each replica and (b) each configurational snapshot computed using normal mode analysis for each of the nine protease inhibitors studied. In the case of the inhibitor lopinavir (LPV) two replica ensembles are shown, the first with open circles and the latter filled triangles. Explanations of the abbreviations used for each drug are given in Table 1. The expected normal distribution given the same mean and standard deviation for each dataset is shown by the blue lines (the distribution for the second LPV replica is shown in red).

Unlike MMPB(GB)SA and normal modes the binding free energy of association, ΔG_{Assoc}, has not previously been widely applied and little is known about the performance of this methodology.

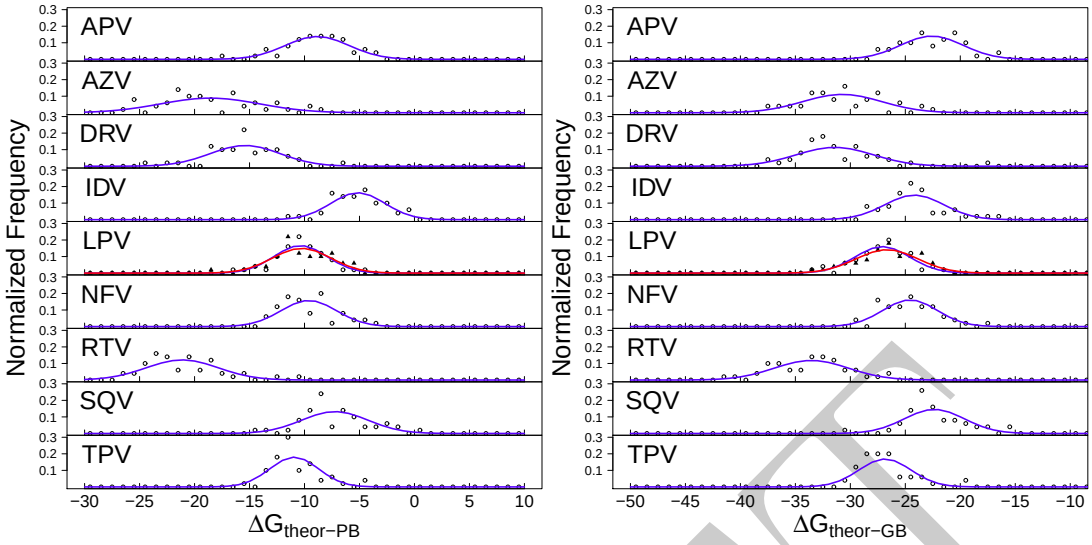

(a) (b)

Figure 6: Normalized frequency distribution analysis of the binding affinities calculated for each replica using (a) MMPBSA and normal mode analysis ($\Delta G_{theor-PB}$) and (b) MMGBSA and normal mode analysis ($\Delta G_{theor-GB}$) for each of the nine protease inhibitors studied. In the case of the inhibitor lopinavir (LPV) two replica ensembles are shown, the first with open circles and the latter filled triangles. The narrowest replica distribution for the ΔG_{MMPBSA} and ΔG_{MMGBSA} results (for NFV and LPV respectively) are 1.5 and 1.6 kcal mol^{-1}. The expected normal distribution given the same mean and standard deviation for each dataset is shown by the blue lines (the distribution for the second LPV replica is shown in red).

Figure 7 shows that we obtain comparatively narrow distributions of the replica averages compared to any of the other free energy components studied here, with a typical range of approximately 5 kcal mol^{-1}. The overall averages also show a relatively small range across the different drugs of only 4.29 kcal mol^{-1} with 6 of the 9 drugs having averages between 11 and 12 kcal mol^{-1} (further details are provided in Table S4). It does not appear from the distributions that ΔG_{Assoc} is well converged for the ensembles used here, suggesting that for this technique more sampling is required. An alternative explanation of the poor approximation to a normal distribution is that the naive implementation of this technique applied here (assuming that each replica represents a single local energy minimum) is inappropriate and that some form of clustering might be used before the calculation is performed.

Overall the results presented here confirm the observation that individual simulation trajectories do not yield reproducible results but that ensembles of simulations can be efficiently used

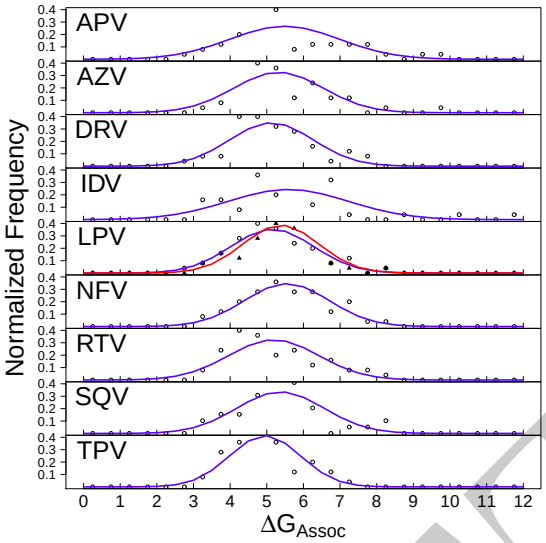

Figure 7: Normalized frequency distribution analysis of the free energy of association (ΔG_{Assoc}) for each replica . The expected normal distribution given the same mean and standard deviation for each dataset is shown by the blue lines (the distribution for the second LPV replica is shown in red).

to generate converged free energy estimates. Thus our findings made previously about lopinavir bound to protease sequences of different binding strengths[13], also apply in the case of the ranking of different protease inhibitors. Remarkably, we observe that the distribution of replica averages of $-T\Delta S_{NM}$ is no broader than that of ΔG_{MMPBSA} or ΔG_{MMGBSA}.

3.2 Comparison with Experimental Data

In order to assess the efficacy of the binding affinity assessment methodologies we have employed it is necessary to compare our results with experimental values. We searched BindingDB[43], an online database of measured binding affinities, to identify datasets which covered all nine FDA approved protease inhibitors under comparable experimental conditions. We found datasets from two groups which fit these criteria, that reported by Freire and coworkers[44–46] (we will refer to this as $Expt1$) and that in Dierynck et al.[47] (we will refer to this as $Expt2$). Two statistical measures are often used to compare computationally derived binding estimates to those from experiment; the coefficient of determination (r^2) and the Spearman rank coefficient (r_s). The former describes the level of linear correlation between the two datasets, the latter whether the rank ordering of the

two datasets is the same. Comparing the two experimental datasets we obtain a r^2 value of 0.47 and a r_s of 0.90, suggesting that whilst the rank ordering of the proteins is consistent the exact differences between ligands varies considerably. Consequently, we decided to use r_s as the main metric to assess the performance of the different free energy methodologies we have employed and to compare our results to both the two experimental datasets and the average of the two (we will refer to the average dataset as *ExptAvg*).

Table 2 details the comparison between free energy estimates computed via MMPBSA (ΔG_{MMPBSA}) and MMGBSA (ΔG_{MMGBSA}) alone and incorporating normal mode derived configurational entropy ($\Delta G_{theor-PB}$ and $\Delta G_{theor-GB}$). The only values to approach accuracy in terms of the absolute binding free energy are from $\Delta G_{theor-PB}$. Even these values are generally more positive (less attractive) than the experimental values; this is consistent with previous observations that the binding of the conserved water molecule contributes between 3 and 4 kcal mol^{-1} to the strength of binding[48–50]. None of the methodologies produce r^2 results higher than 0.57 to the values from *Expt*1, *Expt*2 or *ExptAvg* (see Table 3), with the methods incorporating configurational entropic contribution ($\Delta G_{theor-PB}$ and $\Delta G_{theor-GB}$) generally slightly improving on those that do not (ΔG_{MMPBSA} and ΔG_{MMGBSA}). Graphical comparisons of the computed binding affinities and corresponding experimental values can be found in the Supporting Information.

The binding affinity estimates for two drugs, those for RTV and ATZ, stand out as being much too attractive. It was noted above that these two ligands exhibited the least well behaved replica distributions for all of the free energy calculation components and that they are the largest drugs in the dataset. It is likely that these drugs distort the protein geometry more than is the case for smaller drugs and that there should be an energetic penalty associated with this[51]. The calculations presented here use a single trajectory approach and consequently no account is taken of these potential contributions to the binding affinity (sometimes referred to as 'strain'[21]). Specifically, these larger drugs have more interactions outside the active site (in the sites usually referred to as P3 and P3′ either side of the binding cavity) than are found in other ligands[51]. This region of the protease is made up of residues R8 and P81 of one monomer and G27, A28, D29, D30, G48 and

G49 of the other. It is possible that these interactions stabilize unrepresentative minima in the free energy landscape close to the original crystal structure, which may require additional sampling to escape from compared to simulations of smaller ligands. We investigated the idea that simply increasing the length of each replica might overcome any such barriers by extending 10 replicas of the RTV ensemble to 20 nanoseconds and found that in one case a conformational flip in the D29 residue allowed water access to the drug which was accompanied by a weakening of ΔG_{MMPBSA} estimates of binding strength of approximately 10 to 15 kcal mol^{-1} (see Supporting Information). Our previous work has shown that when RTV is docked into protease conformations taken from LPV simulations a significantly lower binding affinity is obtained than in simulations started from RTV crystal structures[42] (although not by enough to result in a correct ranking with respect to the results obtained for other inhibitors in this study). This phenomenon was observed to be linked to the accessibility of the drug and protease active site to individual water molecules. Oehme et al.[12] have also suggested that the binding strength of larger drugs are over estimated by MMPBSA and MMGBSA, although they did not note any specific interactions as the cause.

Excluding the two larger drugs we obtain much improved rankings as shown in Table 4. The MMPBSA results, both including and excluding $-T\Delta S_{NM}$ provide good agreement with both the $Expt1$ and $Expt2$ datasets as well as the average results $ExptAvg$. Overall the rankings are improved by the addition of configurational entropy. MMGBSA without normal modes performs poorly but the incorporation of $-T\Delta S_{NM}$ renders its performance comparable to MMPBSA without this contribution. Figure 8 indicates that when normal modes are not included in the ranking the relative binding strength for TPV is significantly underestimated compared to the average experimental values for both ΔG_{MMPBSA} and ΔG_{MMGBSA}. The inclusion of the configurational entropy corrects this and allows the tight binding drugs LPV, TPV and DRV to be differentiated from those which are consistently seen to be weaker binders in the two experimental studies. Furthermore, for this set of ligands when normal modes are included in the calculation we significantly improve the coefficient of determination, r^2, (see Table 5) indicating that the differentiation between drugs is more quantitatively accurate. Disappointingly, the inclusion of the free energy of association,

Table 2: Binding affinity estimates for all FDA approved HIV-1 protease inhibitors bound to HXB2 wildtype proteases. Values are shown for MMPBSA (ΔG_{MMPBSA}), MMGBSA (ΔG_{MMGBSA}), normal mode derived configurational entropy ($-T\Delta S_{NM}$) and combined methods ($\Delta G_{theor-PB}$ and $\Delta G_{theor-GB}$). Experimental values from Ohtaka et al.[44], Ohtaka and Freire[45], Velazquez-Campoy et al.[46] and Dierynck et al.[47] are also shown (denoted by $Expt1$, $Expt2$ and $ExptAvg$ respectively).

Drug	ΔG_{MMPBSA}	ΔG_{MMGBSA}	$-T\Delta S_{NM}$	$\Delta G_{theor-PB}$	$\Delta G_{theor-GB}$	ΔG_{Expt1}	ΔG_{Expt2}	$\Delta G_{ExptAvg}$
APV	-41.81 (0.04)	-55.54 (0.03)	32.96 (0.24)	-8.85 (0.28)	-22.58 (0.27)	-13.2 (0.03)	-12.3 (0.12)	-12.7 (0.15)
AZV	-54.06 (0.05)	-66.22 (0.04)	35.48 (0.25)	-18.59 (0.30)	-30.74 (0.29)	-14.2 (0.09)	-12.7 (0.05)	-13.4 (0.14)
DRV	-47.38 (0.04)	-63.39 (0.03)	31.97 (0.24)	-15.41 (0.28)	-31.42 (0.27)	-15.0 (0.09)	-16.6 (0.20)	-15.8 (0.29)
IDV	-42.16 (0.03)	-61.19 (0.02)	37.02 (0.23)	-5.14 (0.26)	-24.17 (0.25)	-12.4 (0.03)	-11.7 (0.23)	-12.1 (0.26)
LPV	-47.68 (0.04)	-64.40 (0.02)	37.31 (0.23)	-10.37 (0.27)	-27.09 (0.25)	-15.1 (0.09)	-13.0 (0.06)	-14.1 (0.15)
LPV 2	-48.38 (0.03)	-64.79 (0.03)	38.13 (0.24)	-10.25 (0.27)	-26.66 (0.27)	-15.1 (0.09)	-13.0 (0.06)	-14.1 (0.15)
NFV	-42.75 (0.03)	-57.71 (0.02)	33.15 (0.24)	-9.60 (0.27)	-24.56 (0.26)	-12.8 (0.05)	-11.5 (0.21)	-12.1 (0.26)
RTV	-58.80 (0.03)	-71.23 (0.03)	37.68 (0.24)	-21.12 (0.27)	-33.55 (0.27)	-13.7 (0.05)	-11.8 (0.10)	-12.7 (0.15)
SQV	-44.17 (0.04)	-59.29 (0.03)	36.93 (0.24)	-7.24 (0.28)	-22.36 (0.27)	-13.0 (0.04)	-12.0 (0.13)	-12.5 (0.17)
TPV	-43.08 (0.03)	-59.00 (0.03)	32.15 (0.24)	-10.93 (0.27)	-26.85 (0.27)	-14.6 (0.09)	-12.5 (0.22)	-13.5 (0.31)

Mean energies are in kcal mol^{-1}. Standard errors are shown in parentheses.

Table 3: Spearman rank coefficient (r_s) for each of the studied computational free energy methodologies compared to the two experimental datasets and their average, ranking all nine FDA approved drugs.

Method	$Expt1$	$Expt2$	$ExptAvg$
ΔG_{MMPBSA}	0.57	0.41	0.48
ΔG_{MMGBSA}	0.46	0.35	0.39
$\Delta G_{theor-PB}$	0.56	0.43	0.56
$\Delta G_{theor-GB}$	0.55	0.43	0.57

ΔG_{Assoc}, has no impact on the quality of the ranking using MMPBSA and makes only a slight improvement for MMGBSA.

The recent work of Oehme et al.[12] examined the ability of MMPBSA and MMGBSA to rank a selection of HIV-1 protease inhibitors (three drugs are common to their work and the present study) using duplicate simulations with similar trajectory lengths to our individual replicas. The range of experimental ΔG values they attempted to evaluate was approximately double that of the difference between DRV and IDV in our chosen test set. The focus of their work was to investigate the impact of ligand parameterization on the free energy values obtained. They found that the Hartree-Fock method employing 6-31G** basis functions which we have used in this study (chosen as it was that used to parameterize the rest of the forcefield we employ) performed particularly poorly; their results produced r^2 values with a magnitude of less than 0.01 for ΔG_{MMPBSA} and $\Delta G_{theor-PB}$, and of 0.60 and 0.50 for ΔG_{MMGBSA} and $\Delta G_{theor-GB}$ respectively. Their results are comparable with our results when we include RTV and AZV. Even given the fact that the differences we aimed to detect were much smaller, we significantly improved on all of the performance metrics through the use of our ensemble approach. It is certainly possible that the choice of ligand parameterization may alter the characteristics of the free energy landscape in such a way that differing levels of sampling are required to correctly converge results. However, it seems unlikely that so large a difference is produced that results from such small numbers of simulations would be reproducible, given the range of values we obtain in our ensemble studies.

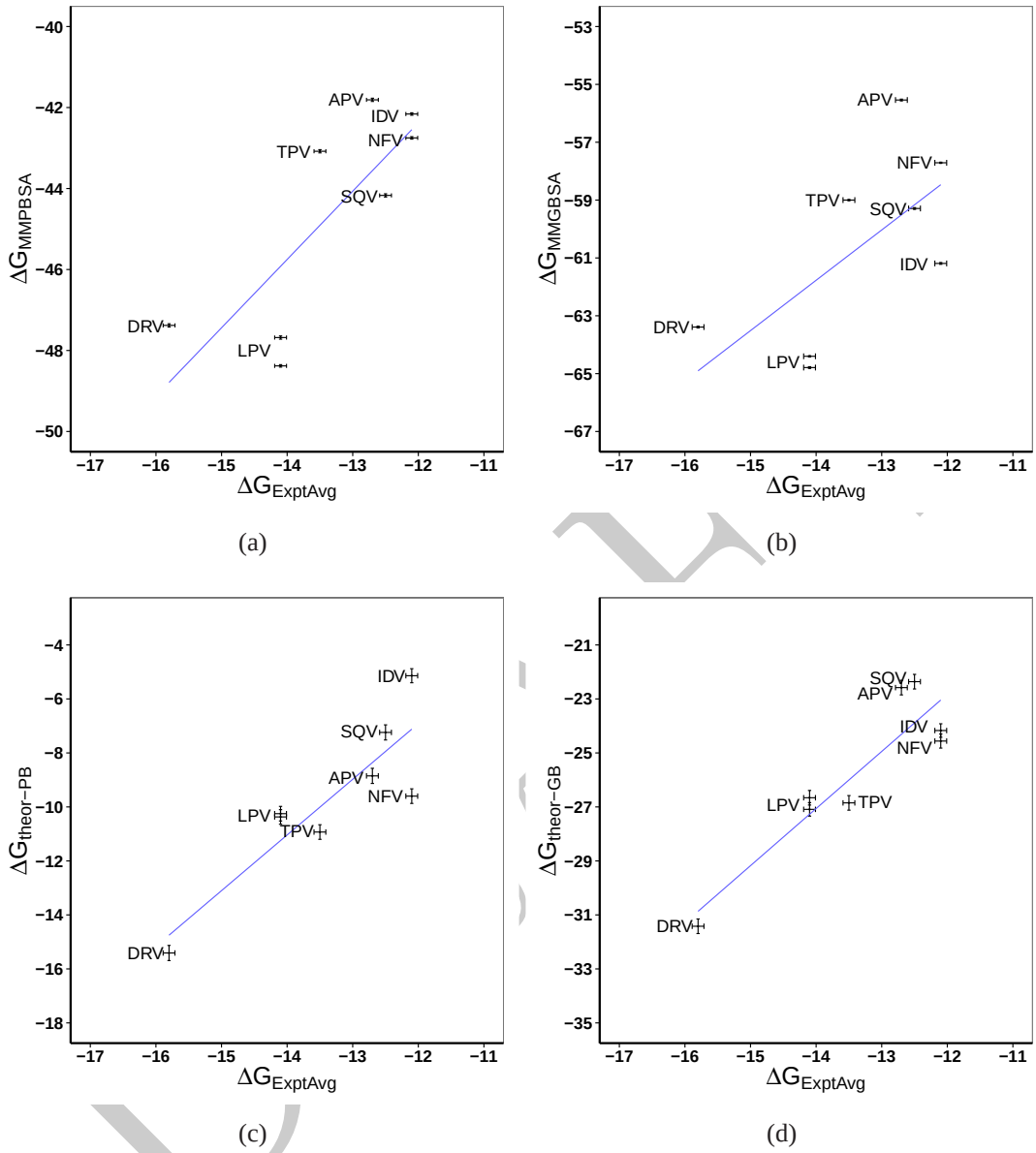

Figure 8: Average experimental absolute binding free energies ($\Delta G_{ExptAvg}$) of wildtype HIV-1 protease bound to seven inhibitors compared with theoretical predictions using (a) MMPBSA (ΔG_{MMPBSA}), (b) MMGBSA (ΔG_{MMGBSA}), (c) MMPBSA and normal mode analysis ($\Delta G_{theor-PB}$) and (d) MMGBSA and normal mode analysis ($\Delta G_{theor-GB}$). Two drugs RTV and ATZ are excluded here due to systematic over estimation of the binding affinity of large ligands. Error bars show the standard errors given in Table 2. The blue line represents a linear regression performed on each data set. Spearman rank coefficients are given in Table 4. There is a clear improvement in the rankings produced upon the inclusion of normal mode entropy estimates.

Table 4: Spearman rank coefficient (r_s) for each of the studied computational free energy methodologies compared to the two experimental datasets and their average.

Method	$Expt1$	$Expt2$	$ExptAvg$
ΔG_{MMPBSA}	0.80	0.71	0.72
ΔG_{MMGBSA}	0.63	0.63	0.60
$\Delta G_{theor-PB}$	0.73	0.78	0.82
$\Delta G_{theor-GB}$	0.67	0.74	0.76
$\Delta G_{PB-Assoc}$	0.80	0.71	0.72
$\Delta G_{GB-Assoc}$	0.68	0.68	0.65

Table 5: Coefficient of determination (r^2) for each of the studied computational free energy methodologies compared to the two experimental datasets and their average.

Method	$Expt1$	$Expt2$	$ExptAvg$
ΔG_{MMPBSA}	0.71	0.39	0.64
ΔG_{MMGBSA}	0.48	0.26	0.44
$\Delta G_{theor-PB}$	0.58	0.74	0.77
$\Delta G_{theor-GB}$	0.61	0.76	0.83
$\Delta G_{PB-Assoc}$	0.74	0.41	0.67
$\Delta G_{GB-Assoc}$	0.52	0.28	0.48

4 Conclusions

In the present work we have assessed the potential of the MMPBSA and MMGBSA methodologies to produce the kind of reliable and reproducible predictions of binding affinity that could be used in drug discovery and personalized medicine applications. We have found that for seven of the nine FDA approved HIV protease inhibitors (amprenavir, darunavir, indinavir, lopinavir, nelfinavir, saquinavir and tipranavir) these methodologies work well, reproducing experimental rankings comparably well to how different experiments correlate to one another.

The two largest ligands in our test set atazanavir and ritonavir are poorly handled by all of the approaches we have applied, illustrating that the MMPBSA and MMGBSA methodologies have significant limitations in the range of ligands that can be consistently compared (at least in the case of the HIV-1 protease). Compared to the well ranked ligands these larger inhibitors have a greater

level of interactions beyond the active site. These interactions distort protein geometry and are poorly handled by the single trajectory approaches which we have employed here. It remains a significant challenge for future work to obtain converged values of the free energy that account for these differences. Our findings also suggest that the optimal sampling strategy and the applicability of the methods will depend strongly on the details of the protein target, with even what may be thought of as peripheral residues potentially having a significant impact on the computed binding affinities.

In order that free energy calculations can be further validated it is necessary that it becomes standard practice to present analysis of the sampling and convergence properties of computations, not merely their results. The MMPBSA and MMGBSA methodologies have different convergence properties, with the latter converging much more quickly and being insensitive to the length of replica simulations in our ensembles. These observations agree with the single simulation results of Srivastava and Sastry[11] in which greater simulation length was seen to improve the ability of MMPBSA to rank ligands but not MMGBSA. However, we observe that there is greater variability in MMPBSA results as they are extended, which suggests that some of the benefits of trajectory elongation observed in that study were fortuitous. Furthermore, our work has suggested that, with sufficient sampling, configurational entropies calculated using normal-mode analysis do exhibit normal distributions, contrary to our previous observations[13]. Normal distributions required us to sample 25 conformations per nanosecond of trajectory. Surprisingly, we observe the distribution of average replica free energy contributions from normal modes to be less broad than that for MMPBSA or MMGBSA.

Within the range of ligands that can be consistently treated we obtain good agreement with experimental drug rankings from MMPBSA alone and from both MMPBSA and MMGBSA with normal mode entropy contributions. MMPBSA with normal mode configurational entropy provides the best statistical reproduction of experimental results as measured by Spearman rank coefficient, with an r^2 value of 0.82 to the average results of the two experimental datasets. Whilst the difference between this method and that excluding configurational entropy is relatively small, the

extra computational effort can be justified by the improvement in coefficient of determination when compared to the average of the two experimental datasets which suggests that it better reproduces the magnitude of binding affinity difference between the ligands. We also investigated the potential of the free energy of association suggested by Swanson et al.[20] to improve rankings but found that this did not enhance any of the rankings obtained using MMPBSA. A small improvement was seen in the MMGBSA results when this contribution was included.

One of the most important factors in the ability to obtain the rankings we have presented is the use of ensemble simulations. The values obtained from ensembles of 50 replica simulations of the same protease - drug complex, differing only in initially assigned atom velocities, varied by as much as 10 kcal mol^{-1}, a greater range than that between the best and worst binding FDA approved inhibitors. The importance of the extensive level of sampling required to obtain consistently converged estimates of binding free energies (irrespective of their accordance with experimental or 'real' values) is perhaps the most striking result of the present study. We have presented distributions of the results of all of the free energy computations we have conducted, and believe that this should become common practice for all future computational binding affinity studies. We hope that future work will provide standards that better allow comparisons of different studies using a range of techniques and simulation parameters.

The aim of this study has been not only to validate the ability of MMPB(GB)SA based free energy calculations to distinguish HIV-1 protease inhibitors but to investigate the broader suitability of the methods for rational drug design and personalized medicine applications. One of the major attractions of MMPB(GB)SA calculations is the promise of general applicability to any chemical species whereas other techniques, such as free energy perturbation (FEP) or thermodynamic integration (TI), are practically limited to considering free energy differences between molecules that are relatively similar. In drug discovery and lead enrichment applications the task is to provide rapid results for libraries of hundreds or thousands of candidate compounds. The computational cost of the ensemble MD simulations that we found necessary to obtain reliable MMPB(GB)SA values meant that at present the use of these techniques in this field is unsuitable. It is likely that for

such applications empirical scoring functions based on quantitative structure-activity relationship (QSAR) models will continue to be the best option (despite the obvious dangers of extrapolating beyond the data used to derive them). In personalized medicine contexts the demands are however quite different, with results typically required only for a limited selection of drugs bound to one or two target protein sequences. We have previously shown how MD simulations could be integrated into clinical decision support systems as part of the ViroLab project[14,52]. Furthermore, the required turn around times of days or up to a week are easily obtainable. Ensemble simulations represent a very time efficient method of running MD calculations as each replica can be run concurrently given sufficient compute resource. The 6 nanoseconds of trajectory for each replica can typically be produced in 15 hours (assuming 2.5 hours per nanosecond using 64 CPU cores based on our experience on several machines) and the free energy analysis within another 12 hours. These times are only likely to reduce as new technology is introduced and algorithmic improvements are implemented.

Combining the results for different inhibitors presented here with our previous demonstration that the MMPBSA methodology with normal modes can successfully and reproducibly estimate the binding affinities of mutant proteases to a single inhibitor[13] we believe that MMPB(GB)SA techniques are capable of making significant contributions in academic reserach as well as basic and clinical medicine.

Acknowledgments

This work has been made possible thanks to computer resources provided by XSEDE TRAC award TG-MCB090174. In particular simulations were performed on the Kraken machine at the National Institute for Computational Infrastructure (NICS) and Ranger at the Texas Advanced Computing Center (TACC). We thank Yaakoub El Khamra (TACC) for exceptional support on Lonestar and Ranger. The authors acknowledge the use of the UCL Legion High Performance Computing Facility (Legion@UCL), and associated support services, in the completion of this work. The work presented here made use of the EMERALD HPC facility provided by the e-Infrastructure South Centre for Innovation (EPSRC Grant ref EP/K000144/1, EP/K000136/1). This work made

use of HECToR, the UK's national high-performance computing service, funded by the Office of Science and Technology through EPSRC's High-End Computing Programme. Access to HECToR was provided through the 2020 Science programme (http://www.2020science.net/, EP/I017909/1). We are grateful to the DEISA Consortium, co-funded through the EU FP6 project RI-031513 and the FP7 project RI-222919, for support within the DEISA Extreme Computing Initiative (DECI) which provided access to the Huygens machine at SARA and HLRB II at Leibniz-Rechenzentrum (LRZ). We thank the SAGA team members – Andre Merzky, Andre Luckow and Ole Weidner – for their support and expertise. Important funding for SAGA was provided by UK EPSRC grant number GR/D0766171/1 (via OMII-UK) and HPCOPS NSF-OCI 0710874. DWW & PVC would also like to thank the EU FP7 CHAIN (HEALTH-2007-2.3.2-7) and FP7 VPH-SHARE (FP7-ICT 269978) projects for their support.

Supporting Information Available

Details of the SAGA and BigJob middleware used to facilitate this study, alongside thermodynamic decomposition of binding affinities, structural and energetic analysis of the extended ritonavir simulations discussed in the main text are provided in Supporting Information. This information is available free of charge via the Internet at `http://pubs.acs.org/`.

References

(1) Walter, F. M.; Emery, J. D. *Br J Gen Pract* **2012**, *62*, 120–121.

(2) Wright, D. W.; Wan, S.; Shublaq, N.; Zasada, S. J.; Coveney, P. V. *Wiley Interdiscip Rev Syst Biol Med* **2012**, *4*, 585–598.

(3) Durrant, J. . D.; McCammon, J. A. *BMC Biol* **2011**, *9*, 71.

(4) Xie, L.; Evangelidis, T.; Xie, L.; Bourne, P. E. *PLoS Comput Biol* **2011**, *7*, e1002037.

(5) Gilson, M. K.; Zhou, H. *Annu Rev Biophys Biomol Struct* **2007**, *36*, 21–42.

(6) Steinbrecher, T.; Labahn, A. *Curr Med Chem* **2010**, *17*, 767–785.

(7) Massova, I.; Kollman, P. *Journal of the American Chemical Society* **1999**, *121*, 8133–8143.

(8) Kollman, P. A.; Massova, I.; Reyes, C.; Kuhn, B.; Huo, S.; Chong, L.; Lee, M.; Lee, T.; Duan, Y.; Wang, W.; Donini, O.; Cieplak, P.; Srinivasan, J.; Case, D. A.; Cheatham, T. E. *Acc Chem Res* **2000**, *33*, 889–897.

(9) Onufriev, A.; Bashford, D.; Case, A. A. *The Journal of Physical Chemistry B* **2000**, *104*, 3712–3720.

(10) Hou, T.; Wang, J.; Li, Y.; Wang, W. *J Chem Inf Model* **2011**, *51*, 69–82.

(11) Srivastava, H. K.; Sastry, G. N. *J Chem Inf Model* **2012**, *52*, 3088–3098.

(12) Oehme, D. P.; Brownlee, R. T. C.; Wilson, D. J. D. *J Comput Chem* **2012**, *33*, 2566–2580.

(13) Sadiq, S. K.; Wright, D. W.; Kenway, O. A.; Coveney, P. V. *J Chem Inf Model* **2010**, *50*, 890–905.

(14) Wright, D. W.; Coveney, P. V. *Journal of Chemical Information and Modeling* **2011**, *51*, 2636–2649.

(15) Wan, S.; Coveney, P. V. *J R Soc Interface* **2011**,

(16) Yun, C.; Boggon, T. J.; Li, Y.; Woo, M. S.; Greulich, H.; Meyerson, M.; Eck, M. J. *Cancer Cell* **2007**, *11*, 217–227.

(17) Kim, Y.; Li, Z.; Apetri, M.; Luo, B.; Settleman, J. E.; Anderson, K. S. *Biochemistry* **2012**, *51*, 5212–5222.

(18) Caves, L. S. D.; Evanseck, J. D.; Karplus, M. *Protein Science* **1998**, *7*, 649–666.

(19) Genheden, S.; Ryde, U. *J Comput Chem* **2010**, *31*, 837–846.

(20) Swanson, J. M. J.; Henchman, R. H.; McCammon, J. A. *Biophys J* **2004**, *86*, 67–74.

(21) Mobley, D. L.; Dill, K. A. *Structure* **2009**, *17*, 489–498.

(22) Pearlman, D. A. *J Med Chem* **2005**, *48*, 7796–7807.

(23) Stoica, I.; Sadiq, S. K.; Coveney, P. V. *Journal of the American Chemical Society* **2008**, *130*, 2639–2648.

(24) Case, D. A.; Cheatham, T. E.; Darden, T.; Gohlke, H.; Luo, R.; Merz, K. M.; Onufriev, A.; Simmerling, C.; Wang, B.; Woods, R. J. *J Comput Chem* **2005**, *26*, 1668–1688.

(25) Rocchia, W.; Sridharan, S.; Nicholls, A.; Alexov, E.; Chiabrera, A.; Honig, B. *J Comput Chem* **2002**, *23*, 128–137.

(26) Sanner, M. F.; Olson, A. J.; Spehner, J. C. *Biopolymers* **1996**, *38*, 305–320.

(27) Singh, N.; Warshel, A. *Proteins* **2010**, *78*, 1705–1723.

(28) Michaud-Agrawal, N.; Denning, E. J.; Woolf, T. B.; Beckstein, O. *J Comput Chem* **2011**,

(29) Liu, P.; Agrafiotis, D. K.; Theobald, D. L. *J Comput Chem* **2010**, *31*, 1561–1563.

(30) Theobald, D. L. *Acta Crystallogr A* **2005**, *61*, 478–480.

(31) Sadiq, S. K.; Wright, D. W.; Watson, S. J.; Zasada, S. J.; Stoica, I.; Coveney, P. *Journal of Chemical Information and Modeling* **2008**, *48*, 1909–1919.

(32) Duan, Y.; Wu., C.; Chowdhury., S.; Lee, M. C.; Xiong, G.; Zhang., W.; Yang, R.; Cieplak, P.; Luo, R.; Lee, T.; Caldwell, J.; Wang, J.; Kollman, P. *J Comput Chem* **2003**, *24*, 1999–2012.

(33) Wang, J.; Wolf, R. M.; Caldwell, J. W.; Kollman, P. A.; Case, D. A. *J Comput Chem* **2004**, *25*, 1157–1174.

(34) O'Boyle, N. M.; Banck, M.; James, C. A.; Morley, C.; Vandermeersch, T.; Hutchison, G. R. *J Cheminform* **2011**, *3*, 33.

(35) Frisch, M. J. et al. Gaussian 98. Gaussian, Inc., 1998.

(36) Phillips, J. C.; Braun, R.; Wang, W.; Gumbart, J.; Tajkhorshid, E.; Villa, E.; Chipot, C.; Skeel, R. D.; Kalé, L.; Schulten, K. *J Comput Chem* **2005**, *26*, 1781–1802.

(37) Luckow, A.; Jha, S. *Cloud Computing Technology and Science, IEEE International Conference on* **2010**, 550–556.

(38) Luckow, A.; Lacinski, L.; Jha, S. SAGA BigJob: An Extensible and Interoperable Pilot-Job Abstraction for Distributed Applications and Systems. 2010; `http://doi.ieeecomputersociety.org/10.1109/CCGRID.2010.91`.

(39) Goodale, T.; Jha, S.; Kaiser, H.; Kielmann, T.; Kleijer, P.; von Laszewski, G.; Lee, C.; Merzky, A.; Rajic, H.; Shalf, J. *Computational Methods in Science and Technology* **2006**, *12*, 7–20.

(40) Wittayanarakul, K.; Hannongbua, S.; Feig, M. *J Comput Chem* **2008**, *29*, 673–685.

(41) Yu, C. *Practical Assessment, Research & Evaluation* **2003**, *8*.

(42) Hall, B. A.; Wright, D. W.; Jha, S.; Coveney, P. V. *Biochemistry* **2012**, *51*, 6487–6489.

(43) Chen, X.; Liu, M.; Gilson, M. K. *Comb Chem High Throughput Screen* **2001**, *4*, 719–725.

(44) Ohtaka, H.; Schön, A.; Freire, E. *Biochemistry* **2003**, *42*, 13659–13666.

(45) Ohtaka, H.; Freire, E. *Prog Biophys Mol Biol* **2005**, *88*, 193–208.

(46) Velazquez-Campoy, A.; Muzammil, S.; Ohtaka, H.; Schön, A.; Vega, S.; Freire, E. *Curr Drug Targets Infect Disord* **2003**, *3*, 311–328.

(47) Dierynck, I.; De Wit, M.; Gustin, E.; Keuleers, I.; Vandersmissen, J.; Hallenberger, S.; Hertogs, K. *J Virol* **2007**, *81*, 13845–13851.

(48) Fornabaio, M.; Spyrakis, F.; Mozzarelli, A.; Cozzini, P.; Abraham, D. J.; Kellogg, G. E. *J Med Chem* **2004**, *47*, 4507–4516.

(49) Hamelberg, D.; McCammon, J. A. *J Am Chem Soc* **2004**, *126*, 7683–7689.

(50) Lu, Y.; Yang, C.; Wang, S. *J Am Chem Soc* **2006**, *128*, 11830–11839.

(51) Ali, A.; Bandaranayake, R. M.; Cai, Y.; King, N. M.; Kolli, M.; Mittal, S.; Murzycki, J. F.; Nalam, M. N. L.; Nalivaika, E. A.; Ozen, A.; Prabu-Jeyabalan, M. M.; Thayer, K.; Schiffer, C. A. *Viruses* **2010**, *2*, 2509–2535.

(52) Sloot, P. M. A.; Coveney, P. V.; Ertaylan, G.; Müller, V.; Boucher, C. A.; Bubak, M. *Phil. Trans. R. Soc. A* **2009**, *367*, 2691–2703.